UNIVERSITY OF CALIFORNIA SAN DIEGO

Sortase Labeling eIF4E: A tool to visualize the closed-loop mRNA model

A thesis submitted in partial satisfaction of the requirements
for the degree Master of Science

in

Biology

by

Justin Pi

Committee in charge:

Professor Simpson Joseph, Chair
Professor Yunde Zhao, Co-Chair
Professor Stephanie Mel

2022

The Thesis of Justin Pi is approved, and it is acceptable in quality and form for publication on microfilm and electronically

University of California San Diego

2022

TABLE OF CONTENTS

LIST OF FIGURES

ACKNOWLEDGEMENTS

I am grateful to Professor Joseph for all his support and graciousness in the years working in his lab, taking me in initially as an undergraduate student. As an extremely kind and patient mentor, he has made the hardships of science much more bearable.

I would also like to thank all the members of the Joseph lab for welcoming me in and helping me along my journey. I would like to especially thank Alberto Pequeno, who was my primary mentor and taught me many skills that I have today. Without his help, I would not be where I am today.

I would like to thank my family, who although were over 300 miles away, were always there to support me. I would like to thank my roommates who were always there with me and supported me outside of my scientific endeavors. Finally, I would like to thank Annette, who has been with me throughout all the hardships, as well as accomplishments throughout my academic journey. I am eternally grateful to all these people who have helped shape me into the scientist and human that I am today

ABSTRACT OF THE THESIS

Sortase Labeling eIF4E: A tool to visualize the closed-loop mRNA model

by

Justin Pi

Master of Science in Biology

University of California San Diego, 2022

Professor Simpson Joseph, Chair
Professor Yunde Zhao, Co-Chair

Eukaryotic translation initiation is a highly conserved and regulated biological process. Part of what make translation initiation so complex is the requirement of many proteins to work synergistically. The formation of the mRNA ● eIF4E ● eIF4G ● PABP complex is an essential step in eukaryotic translation. These proteins are often the target of viral infections and when unregulated, can lead to the proliferation of cancers. Therefore, scientists are eager to study the interactions between these proteins to combat and prevent viral infections and diseases.

The mRNA ● eIF4E ● eIF4G ● PABP complex forms the mRNA closed-loop model, where the mRNA will circularize and bring the 5’ and 3’ ends into proximity. The binding of the proteins has been well established. In addition, the formation of a circular mRNA has been visualized by atomic force microscopy in yeast cells. However, the formation of the mRNA closed-loop has not been directly observed in solution with human initiation factors.

Therefore, we have developed a method of labeling eIF4E with a fluorescent dye to visualize the formation of the closed-loop model and study its dynamics. We demonstrate that this labeled eIF4E has a similar biological function to wild-type eIF4E, and can quench the emission of a fluorescent dye attached to the 3’ end of short mRNAs, but not long mRNA’s. This suggests that eIF4E can be used to monitor the proximity of the 5’ and 3’ ends. Finally, we are also able to monitor the assembly of the complex through gel-shift assays.

Chapter 1: Introduction

1.1: Eukaryotic Translation

The translation of messenger RNA to proteins is a highly conserved and universal process observed in all living things. In eukaryotic cells, the initiation of this process is far more complex compared to prokaryotic cells, due to the multitude of proteins and complexes that are required[1]. Eukaryotic cells use two main mechanisms of translation: cap-dependent translation and cap-independent translation[1]. Cap-dependent translation recognizes the 7-methylguanosine cap in the 5' region of eukaryotic mRNA[2]. Eukaryotic cells primarily use cap-dependent translation, but in certain circumstances such as cellular stress or viral infection, these cells will undergo another mechanism of translation, cap-independent translation[2]. Cap-independent translation uses an internal ribosome entry site (IRES) in the mRNA, which recruits the ribosome without the recognition and binding of the cap[1]. Cap-independent translation, however, is overshadowed by cap-dependent translation, a more common and efficient process[1].

Cap-dependent translation begins when the eukaryotic initiation factor 2 (eIF2), guanosine triphosphate, and methionine initiator transfer RNA (Met-tRNAi) assemble into the ternary complex[3]. Afterwards, the ternary complex is recruited to the 40S subunit of the ribosome to form the 43S preinitiation complex (PIC)[3]. Once the 43S preinitiation complex has formed, the eukaryotic initiation factor 4F (eIF4F) complex will recruit the 5' capped mRNA and assemble with the PIC[4]. This newly assembled complex can now start scanning for the AUG start codon and begin the translation of

RNA to amino acids[4]. Within the assembled complex, the eIF4F complex plays a critical role in ensuring translation initiation.

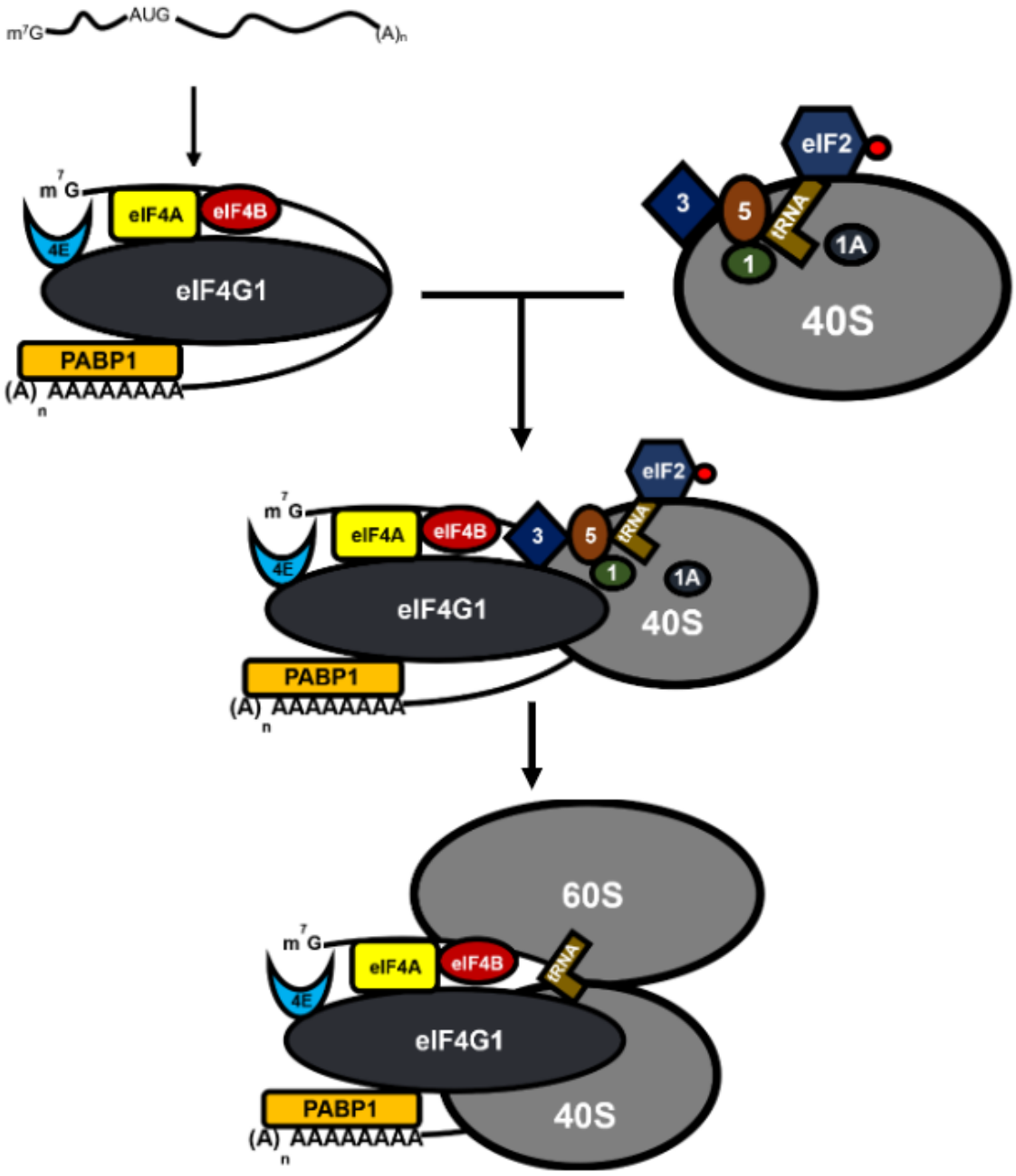

Figure 1.1. Translation Initiation. Schematic diagram showing the proteins of interest in the key steps of translation initiation. Small red circle represents GTP. eIF1, eIF1A, eIF5, eIF3, and eIF4E are labeled without “eIF” within the diagram. Used with permission by Pequeno.

1.2: The eIF4F Complex

The eIF4F complex contains three proteins, eIF4A, eIF4G, and eIF4E, where each protein plays a unique role that ensures translation initiation[4]. As a helicase protein, eIF4A unwinds the secondary structure of capped mRNA for easier access and recruitment of the preinitiation complex[5]. The elucidation of the crystal structure of eIF4A reveals the protein's ability to disrupt protein-RNA interactions within the 5' UTR[6].

eIF4E, The Cap-binding protein

eIF4E is the pivotal cap-binding protein that binds to the 5' cap of mRNA, using two tryptophans to trap the cap and form the PIC, allowing for the initiation of translation[1]. The mechanistic target of rapamycin (mTOR) is a kinase that has a multitude of downstream targets; it contains two catalytic subunits - mTORC1 and mTORC2[7]. mTORC1 regulates multiple cellular processes including protein synthesis and cell growth[8]. mTORC1 binds to 4E binding protein 1 (4EBP-1) and can control the level of phosphorylation of 4EBP-1[7]. Under hypophosphorylation, 4EBP-1 binds to eIF4E and inhibits eIF4E's ability to bind to eIF4G, preventing the assembly of the eIF4F complex and reducing translation. However, when hyperphosphorylated, 4EBP-1 disassembles from eIF4E, and eIF4E can bind to eIF4G again reinitiate tranlation[9]. In addition, phosphorylation of eIF4E can regulate its ability to control translation. eIF4G can recruit Mnk-1, a kinase that phosphorylates eIF4E at the serine 209 position. Once phosphorylated, eIF4E increases the translation of proteins[10]. Both phosphorylation and overexpression of eIF4E have been shown to be oncogenic and a significant contributor

to various cancers[11-17]. Because eIF4E is such a powerful regulator of translation, scientists are eager to study the regulation of this protein and its downstream effects.

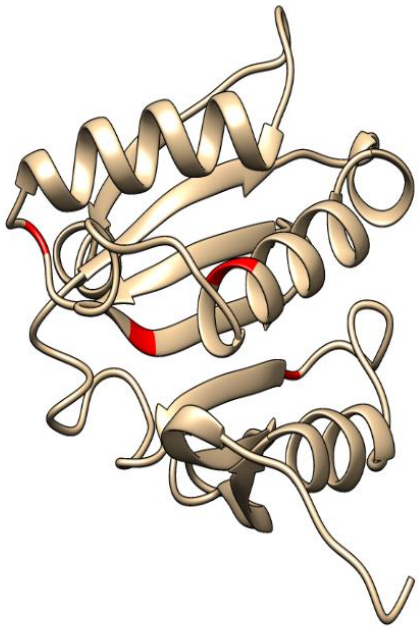

Figure 1.2. Crystal structure of eIF4E. Structure of eIF4E with four cysteines highlighted in red. Structure obtained from PDB accession number 5T46, edited with ChimeraX.

eIF4G, The Scaffolding Protein

eIF4G is a large scaffolding protein that maintains the structural integrity of the eIF4F complex[1]. As an intrinsically disordered protein, only a few fragments of this protein have been purified and their structures solved by x-ray crystallography[3]. Within the eIF4F complex, eIF4G binds to eIF4E and eIF4A[3,18,19]. eIF4G also binds to eIF3, a complex that assists in the assembly of the pre-initiation complex[20]. In the middle portion of the protein, eIF4G contains two RNA domain binding regions (RBD) that allow various RNA's to bind to eIF4G, including viral RNA's[21,22]. eIF4G also possesses a C-

terminal region that binds to Mnk-1, a kinase responsible for phosphorylating eIF4E[10]. Finally, the N-terminal region of eIF4G binds to the poly-adenylate binding protein (PABP1), a protein that binds to the poly-A tail of mRNA[23-25].

Figure 1.3. Architecture of eIF4G. eIF4G and its approximate binding sites.

Because of eIF4G's importance in translation, it can influence many biological processes. When bound to eIF4G, eIF4E has an increased affinity to capped mRNA[26,27]. Reducing the interactions between these proteins has been shown to restore the balance of protein synthesis in Fragile-X syndrome, impair coronavirus replication, and even enhance sensitivity to chemotherapeutic drugs[28-30]. eIF4G can also enhance eIF4A's helicase activity when complexed together[31]. eIF4G in complex with eIF4A is a target of the internal ribosomal entry site (IRES) of the Encephalomyocarditis Virus (EMCV)[32]. This signifies eIF4G's importance in not only cap-dependent translation, but also the cap-independent translation of viruses. Clearly, eIF4G plays an important role in maintaining homeostasis through its interactions.

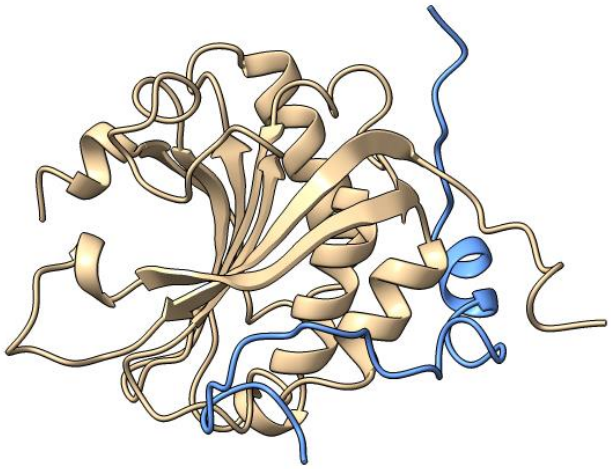

Figure 1.4. Crystal Structure of eIF4G bound to eIF4E. Crystal structure of eIF4G fragment (light blue) bound to eIF4E (tan). PDB accession number 5T46.

1.3: Poly-A Binding Protein

PABP is an RNA-binding protein that is extremely conserved among canonical translation. A 70 kD protein, PABP contains RNA recognition motifs (RRM), which allows the protein to bind to various RNA's[33-35]. In canonical translation, PABP binds to the poly-A tail of mRNA. However, recent studies have shown that viral RNA can also bind to PABP and stimulate translation, bypassing cap-dependent translation[36,37]. In addition, it has been shown that cell extracts lacking PABP have markedly decreased translation, and impaired interactions between eIF4E and eIF4G[38]. Evidently, PABP is an extremely important protein in regulating translation. Along with the eIF4F complex, PABP interacts with mRNA and forms a protein-RNA complex well known as the mRNA closed-loop model.

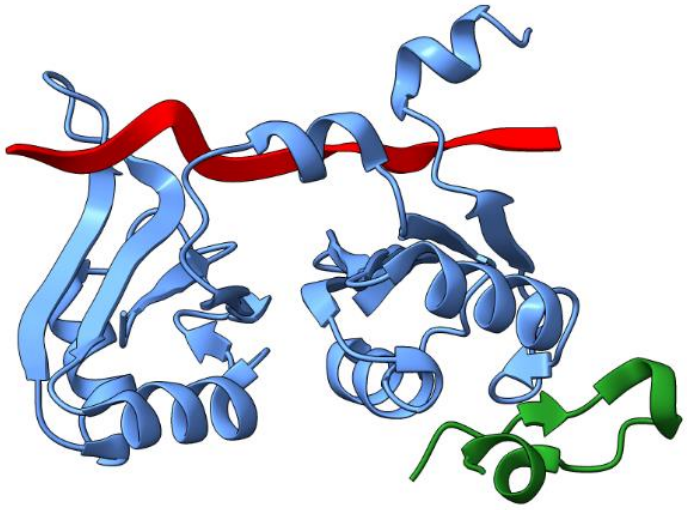

Figure 1.5. Crystal Structure of PABP bound to eIF4G and RNA. RRM1 domain of PABP (light blue) binding to poly-A RNA (red) and eIF4G fragment (green). Accession number 4F02. Edited with ChimeraX

1.4: The mRNA Closed-loop Model

The mRNA closed-loop model is a universally accepted model that is pivotal to understanding more about translation initiation. The model proposes that when eIF4G, PABP, and eIF4E assemble along with capped and tailed mRNA, the mRNA circularizes and brings the 5' and 3' ends within proximity of each other[39-41]. Just like the eIF4F complex, proteins within the closed-loop model interact with each other synergistically. eIF4E, when in complex with both or either eIF4G or PABP, has an increased affinity to the 5' cap[35,38,39,42,43].

There is strong evidence supporting the mRNA closed-loop model, but there is still much to be explored within it. The first evidence of the circularization of the mRNA has been shown in atomic force microscopy of yeast models[41]. In addition, the

circularization of polyribosomes has been observed through cryo-electron microscopy and electron microscopy in wheat-germ extracts[44,45]. Previous studies have also shown preferential proximity of the 5’ and 3’ end in different types of RNA[46,47]. However, the closed-loop mRNA model has not been observed in solution with human initiation translation factors. In addition, little is known about the dynamics of the model – is it a dynamic model that constantly changes? Or is it an extremely stable complex?[40].

The proteins within this complex are extremely influential in the determination of translation. Therefore, they are often targets of therapeutic drugs to treat and prevent cancers and viral infections[48]. We want to understand more about this model and create a tool to visualize the closed-loop mRNA model.

Chapter 2: Results and Discussion

2.1: Testing of Single Cysteine eIF4E constructs

Our goal was to fluorescently label eIF4E. A common way of labeling proteins is through cysteine residues[49]. Therefore, our first plan was to label eIF4E with a fluorescent dye through its cysteine residues. However, eIF4E contains four cysteines, on amino acids 89, 136, 150, and 170 (Figure 1.4, 2.1). To best conduct binding assays, we wanted to have a mono-labeled protein. As a result, we made four single-cysteine constructs, where each eIF4E construct had a single cysteine residue. We mutated the other cysteine residues into serine because it was the most structurally similar amino acid and would hopefully maintain the stability of the protein. Before making these mutant constructs, ChimeraX was used to visualize the crystal structure and determine that the cysteines did not make disulfide bridges.

When purifying the four single-cysteine constructs, the proteins expressed poorly compared to wild-type eIF4E. It seems that making three amino acid mutations affects the expression and integrity of the protein. Out of the four single-cysteine (SC) constructs, only two of them were successfully purified: single-cysteine mutant 136 (SC136), and single-cysteine mutant 150 (SC150).

Before we fluorescently labeled the single-cysteine constructs, we needed to test their ability to bind to capped mRNA. To do so, we used a gel-shift assay, or more specifically, electrophoretic mobility shift assay (EMSA). Much like a DNA gel, the negatively charged RNA will run towards the positive anode of the current. When proteins are bound to the RNA, the RNA-complex will travel differently leading to a

discernable shift[50]. In this case, we used an 18-nucleotide mRNA (S17) that is capped and labeled with fluorescein (FL) in our binding studies (Figure 2.1A).

The EMSA's show that the single-cysteine constructs have poor binding affinity to capped mRNA compared to wild-type eIF4E. When wild-type eIF4E is added to capped S17-FL, a shift is observed (Figure 2.1B). However, when SC136 is added to capped S17-FL, only a faint shifted band is observed. A majority of the capped mRNA is unbound and unshifted, similarly to the band in lane 1 (Figure 2.1B). Evidently, SC136 has a poor binding affinity to capped mRNA. The same observation is shown in the SC150 as well (Figure 2.1C).

Even though disulfide bridges are not predicted within the crystal structure, it seems that the cysteines are still essential in maintaining the integrity of the protein's ability to bind to capped mRNA. Disulfide bridges may in fact be present within eIF4E, or the mutations of the cysteines could change the charge of the protein and disrupt its structure.

When eIF4G is added with eIF4E and S17-FL, eIF4G seems to rescue the single-cysteine constructs' ability to bind to capped mRNA. A super-shift is observed when eIF4G is added in addition to wild-type eIF4E; the visualized RNA migrates less. This is indicative of eIF4G binding to eIF4E, forming the mRNA ● eIF4E ● eIF4G complex. We xare using an eIF4G construct (amino acids 88-653) that does not bind to RNA, shown in lane 4 (Figure 2.1B-C). Therefore, we are confident that the super-shift observed is not from eIF4G binding to the RNA, but of eIF4G binding to eIF4E. In lane 5, we observe the mRNA ● eIF4E ● eIF4G complex with wild-type eIF4E (Figure 2.1B-C). Since we have seen that SC150 and SC136 have poor binding to capped mRNA,

we expect to see poor formation of the mRNA ● SC150/136 ● eIF4G complex as well. Interestingly, when we add eIF4G to the single-cysteine constructs and mRNA, a full shift is observed, with little to no unbound RNA. There appears to be no discernable difference between the wild-type eIF4E and single-cysteine eIF4E mRNA-protein complex (Figure 2.1B-C). This supports previous literature that eIF4G can increase the binding affinity of eIF4E to capped mRNA[26,27]. Our single-cysteine constructs may lack the structural integrity to bind to capped mRNA, but eIF4G could help refold or maintain the integrity of the protein, allowing the mutants to fully bind to capped mRNA once again.

By performing fluorescent anisotropy, we can determine the dissociation constants (K_D) of eIF4E binding to capped mRNA. The K_D of wild-type eIF4E to capped mRNA was determined to be 11.1 ± 1.7 nM, which is significantly lower than the previously reported K_d values[51-53]. Since we observe a weaker binding affinity of the single-cysteine constructs to capped mRNA, we can expect a higher K_D value. A lower K_D value indicates a tighter binding affinity between the capped mRNA and eIF4E. The K_D of SC136 and SC150, respectively, are 37.1 ± 7.1 nM and 138.1 ± 29.4 nM. The SC mutants have around a 4-to-13-fold increase in their K_D relative to wild-type eIF4E, indicating their significantly impaired ability to bind to the 5’ cap. Our gel-shift assays and fluorescent anisotropy assays show that the single-cysteine constructs have a poor binding affinity to capped mRNA compared to wild-type eIF4E. Therefore, we had to develop an alternative method of labeling eIF4E to ensure that the structure and the activity of the protein are unimpaired.

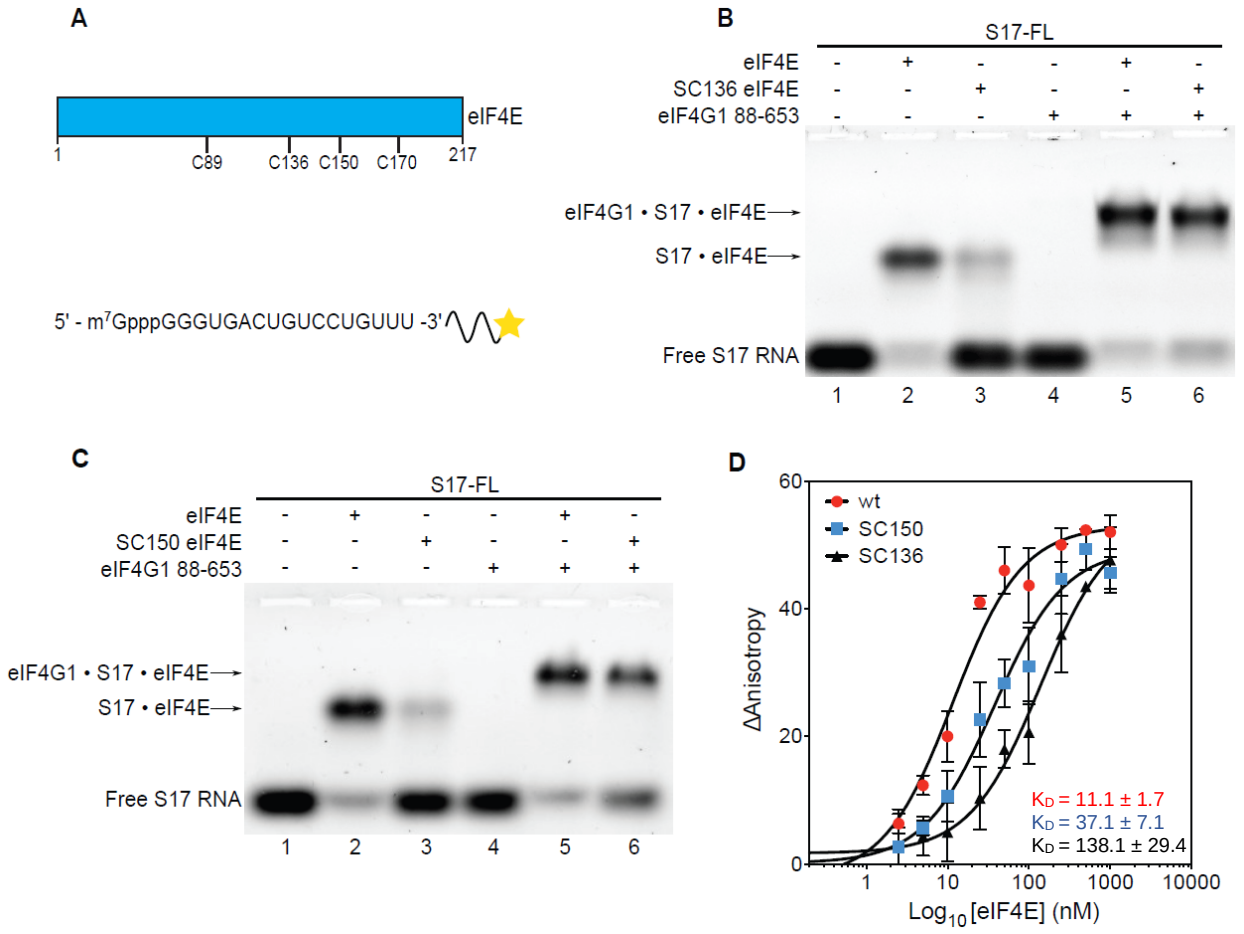

Figure 2.1. Single-cysteine constructs have poor binding affinity to capped mRNA compared to wild-type eIF4E. (A) Schematic of eIF4E showing location of four cysteines, as well as the capped and tailed S17 labeled with fluorescein used in gel-shift assay. (B) Gel-shift assay with SC136. A concentration of 50 nM S17-FL was used, and 500 nM for eIF4G and SC136. (C) Gel-shift assay with SC150. Same conditions were used as (B). (D) Fluorescent anisotropy of eIF4E constructs to capped mRNA. A 1 nM concentration of S17-FL was titrated with an increasing concentration of eIF4E. Dissociation constants (K_D) for wild-type eIF4E, SC136, and SC150 were, respectively, 11.1 ± 1.7 nM, 37.1 ± 7.1 nM, and 138.1 ± 29.4 nM.

2.2: Sortase technology to C-terminally label proteins

Because our single cysteine constructs of eIF4E have poor binding affinity to capped mRNA, we had to develop an alternative method of fluorescently labeling eIF4E. Eventually, we decided upon using the sortase enzyme to specifically label our protein.

The sortase enzyme is a transpeptidase that is commonly expressed within the cell envelope of Gram-positive bacteria[54-56]. In these gram-positive bacteria, the sortase enzyme serves to catalyze and anchor surface proteins onto the peptidoglycan layer of the cell wall[55-57]. An LPXTG amino acid motif (leucine-proline-X-threonine-glycine) on a protein is recognized by the sortase enzyme, which in the presence of calcium, will cleave between the threonine and glycine and form a thioester acyl-intermediate[55,56]. Afterwards, a free amino group on the protein of the cell wall will nucleophilically attack the acyl-intermediate, releasing the sortase enzyme and forming a strong, amide bond[55,56]. Due to its high specificity, the sortase enzyme has been adapted to be used in protein biochemistry and in forming different conjugations[54,57,58].

Multiple advances have allowed the sortase enzyme to be more robust and efficient, allowing this enzyme to be much more applicable in protein biochemistry[54,57,59]. For example, amino acid mutations have increased the sortase enzyme's binding affinity to the LPXTG motif by approximately 120-fold[54]. In addition, single point mutations of E105 and E108 have allowed the sortase enzyme to catalyze independent of the calcium ion[59]. There are two main methods of sortase protein labeling, either through C-terminal labeling or N-terminal labeling[58,60]. In this case, we decided upon C-terminal labeling where eIF4E contains the LPXTG motif, and an oligo-glycine peptide

(sequence GGGGC) labeled with tetramethylrhodamine (TMR) will serve as the nucleophile.

There are certain conditions that must be met for efficient sortase labeling. Through PCR, we inserted a polyglycine linker at the C-terminus end, followed by the LPXTG motif and six histidines (Figure 2.2C). The polyglycine linker provides flexibility to ensure the LPXTG motif is accessible to the sortase enzyme, and the histidines are used for the Ni-NTA purification of the protein[55]. In addition, any unlabeled protein will still have the histidine tag, allowing an effective way of removing any unlabeled protein[55] (Figure 2.2C).

2.3: C-terminal modification of eIF4E for Sortase labeling reaction

Before labeling eIF4E with the sortase enzyme, we wanted to test the binding ability of C-terminally modified construct to capped mRNA. Just as with the SC mutants, we used EMSA's and fluorescent anisotropy to determine the binding affinity of this eIF4E construct to capped mRNA. From the gel-shift assay, the eIF4E with the C-terminal modification (eIF4E-SSM) completely shifts upwards in the presence of capped mRNA, just like wild-type eIF4E (Figure 2.2A). One interesting observation is that the mRNA ● eIF4E-SSM complex has a slightly higher migration than the mRNA ● eIF4E complex. The slightly higher migration could be due to the C-terminal extension of eIF4E-SSM – the larger protein size could cause the slower migration of the protein-mRNA complex. With the addition of eIF4G, the mRNA ● eIF4E-SSM complex super-shifts to form the mRNA ● eIF4E-SSM ● eIF4G complex (Figure 2.2A). Our eIF4E-SSM

binds to eIF4G, similarly to wild-type eIF4E. Therefore, the C-terminal modification seems to not affect the binding ability of eIF4E-SSM to capped mRNA or eIF4G.

Our fluorescent anisotropy assay confirms that the C-terminal modification does not hinder eIF4E-SSM's ability to bind to capped mRNA. The K_D, or dissociation constant of eIF4E-SSM to capped mRNA was 5.5 ± 0.8 nM. Because the K_D of wild-type eIF4E and eIF4E-SSM are very similar, we can be confident that the C-terminal extension of eIF4E does not hinder its ability to bind to capped mRNA. Therefore, we can proceed to fluorescently label eIF4E with the sortase enzyme.

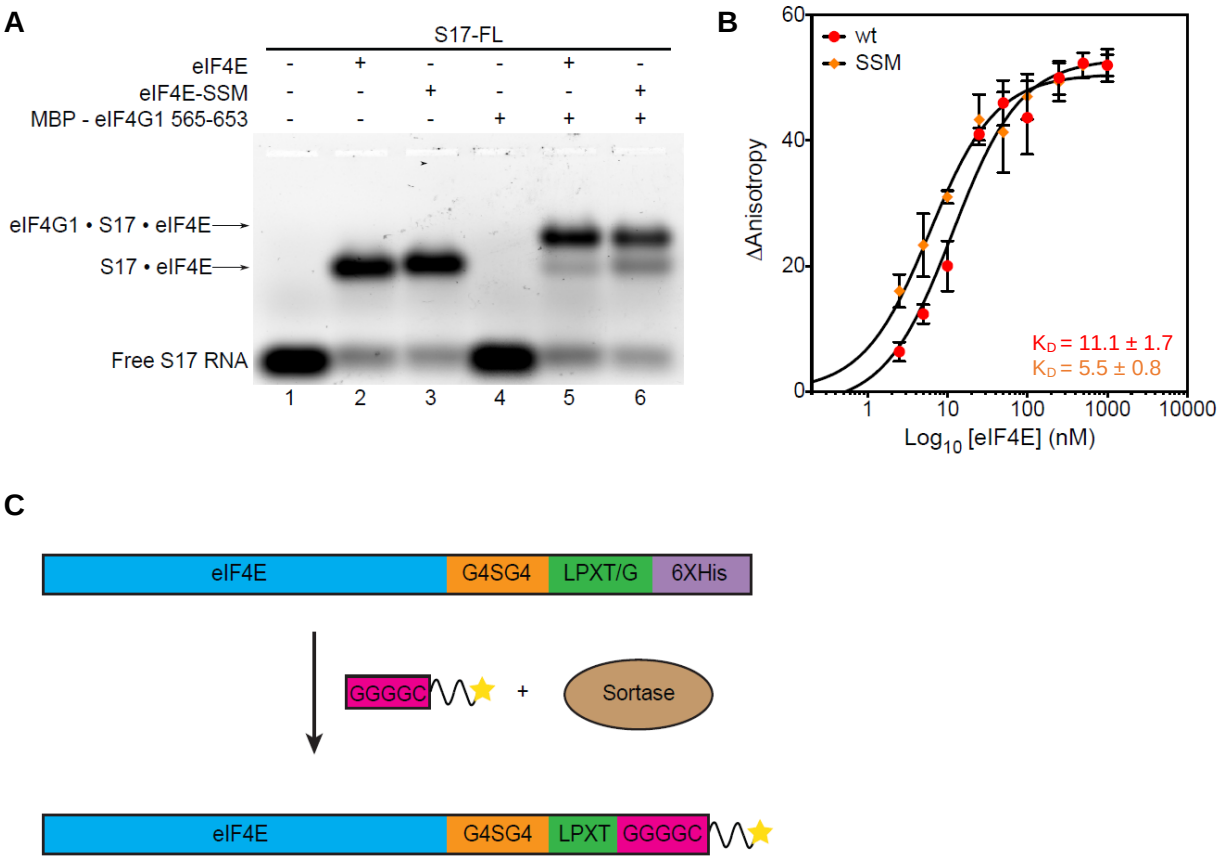

Figure 2.2. C-terminal modification of eIF4E does not hinder eIF4E's ability to bind to capped mRNA. (A) Gel-shift assay with eIF4E-SSM and wild-type eIF4E. A 50 nM S17-FL was used with 500 nM eIF4E and eIF4G. (B) Fluorescent anisotropy of eIF4E and eIF4E-SSM to capped mRNA. A 1 nM S17-FL was titrated with an increasing concentration of eIF4E to obtain a binding curve. K_D of wild-type and eIF4E-SSM binding to capped mRNA, respectively, are 11.1 ± 1.7 nM and 5.5 ± 0.8 nM.

2.4: Fluorescently Labeling eIF4E with the Sortase Enzyme

Now that we were confident that the C-terminal extension does not affect eIF4E's ability to bind to capped mRNA, we proceeded to fluorescently label eIF4E with the sortase enzyme. The labeled peptide is an essential component that will fluorescently label eIF4E. Therefore, it was important to ensure the purity of the peptide. A peptide with the sequence GGGGC was labeled with tetramethylrhodamine (TMR), and successfully purified with an HPLC (Figure 2.3A). With the peptide successfully purified, we proceeded to label eIF4E with the sortase enzyme.

A series of controls were run alongside the sortase reaction to validate our labeling reaction (Figure 2.3B). Our goal was to ensure that eIF4E was specifically labeled from the sortase reaction. As shown in lane 4, the labeled peptide did not fluorescently label eIF4E (Figure 2.3B). Only with the addition of the sortase enzyme, eIF4E is fluorescently labeled (Lane 5, Figure 2.3B). Therefore, we have successfully labeled eIF4E at the C-terminal end with the sortase enzyme. The high specificity of the sortase reaction allows us to have a mono-labeled protein regardless of the number of cysteine residues.

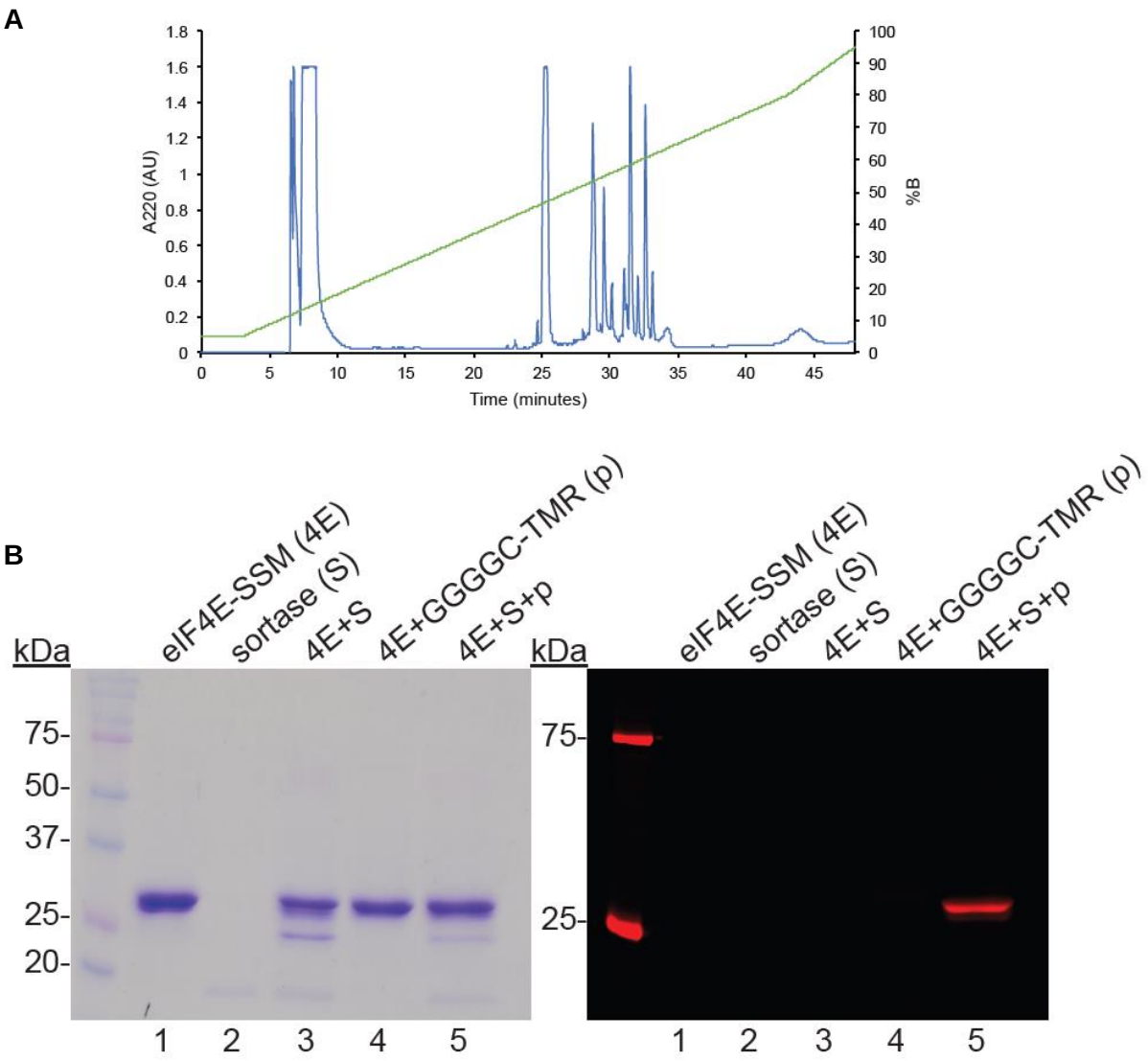

Figure 2.3. Sortase enzyme fluorescently labels the C-terminal end of eIF4E. (A) A chromatogram of the purification of the GGGGC-TMR peptide. Peptide was eluted around 25 minutes in a Vydac C18 column. (B) SDS-PAGE gel of sortase enzyme reaction with controls. Gel was first scanned on Amersham Typhoon, visualizing TMR to see the labeled protein, then stained with Coomasie blue dye.

2.5: S17-FL is quenched by eIF4E-TMR, but CRC1-FL is not

One of the initial experiments that we wanted to test with our fluorescently labeled eIF4E was to test binding to fluorescently labeled mRNA. TMR was the chosen dye because Fluorescein and TMR are FRET (Förster resonance energy transfer) pairs. FRET is a physical phenomenon that is observed when an excited fluorophore transfers its energy to another fluorophore[61-63]. During FRET, a donor fluorophore is excited at a certain wavelength. Once excited, the fluorophore will emit its emission wavelength. If the donor fluorophore is close enough to the acceptor fluorophore, the acceptor fluorophore will be excited by the donor and emit the wavelength of the acceptor fluorophore[61,62]. Therefore, if FRET is occurring, we will see the emission of the acceptor fluorophore by excitation of the donor fluorophore. The main constraints of FRET are proximity and the properly chosen fluorescent pairs[61-63].

For this physical phenomenon to be observed, the two fluorophores must be within proximity of each other. 10 to 100 angstroms is the general range where FRET is observed[61]. In addition, the donor and acceptor fluorescent dye pairs must be chosen correctly. The donor's emission range must overlap with the acceptor's excitation range[61-63]. Only then, can the transfer of energy occur. Because FRET is distant-dependent, this powerful technique has been used to look at binding interactions, cell localization, and cellular processes[62,63].

Using our fluorescently labeled protein and mRNA, we hope to see FRET occurring. When we run the protein ● mRNA complex on a gel-shift assay, we made an interesting observation. The intensity of the labeled eIF4E (eIF4E-TMR) ● S17-FL complex (lane 3) is significantly decreased compared to the wild-type eIF4E ● S17-FL

complex in lane 2 (Figure 2.5A). This may suggest that eIF4E-TMR has not fully bound to the capped mRNA, similarly to the single-cysteine constructs. However, there is little to no difference in unshifted mRNA between wild-type eIF4E and eIF4E-TMR, suggesting the capped mRNA is fully bound to eIF4E-TMR.

The quenching phenomenon observed in lanes 2 and 3 of figure 2.5A can be explained by the proximity of the 5' and 3' end. The 5' cap binds near the C-terminal end of eIF4E (Figure 2.4). Conveniently, our fluorescent dye is positioned at the C-terminal end. Because S17 is a short mRNA with 18 nucleotides, the fluorescein dye on the 3' may be within proximity of the TMR dye of eIF4E. Using ChimeraX, we estimated the distance between the C-terminus end and the 5' cap to be about 20 angstroms (Figure 2.4). Given the small distance and our small mRNA, we can safely assume that our fluorescent dyes will be in proximity to transfer energy. Using a fluorescein emission scan, we can also see the quenching of the 3' fluorescein dye from eIF4E-TMR (Figure 2.5B).

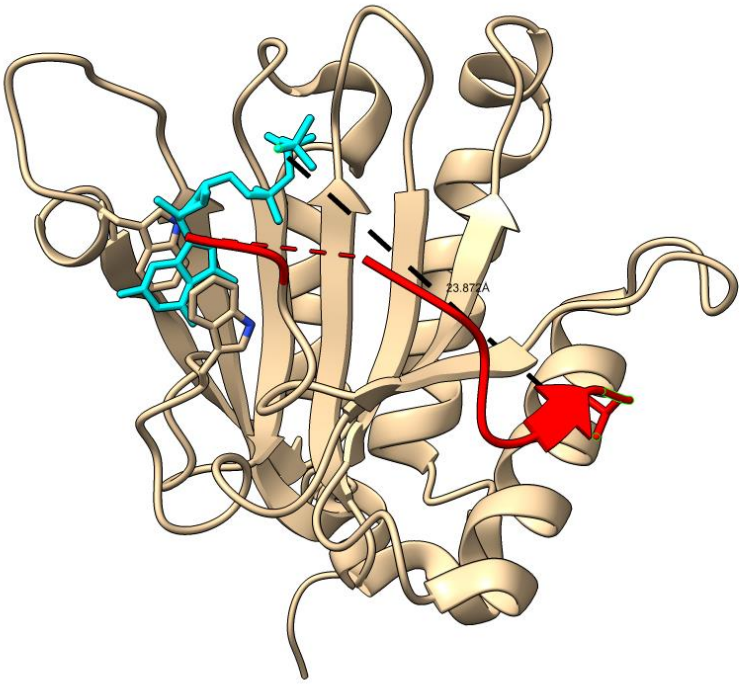

Figure 2.4. Crystal structure of eIF4E binding to m^7G cap. eIF4E (tan) binding to a cap analog (m^7G) colored in cyan. The C-terminal end is labeled in red. The distance between the C-terminus and the cap is approximately 23 angstroms. PDB accession number 1IPC. Edited with ChimeraX.

When S17-FL binds to eIF4E-TMR, a significant quenching occurs; however, FRET is not observed. The labeled mRNA is excited with a wavelength of 465 nM, and the emission scan can be used to observe the relative intensities of each complex. When S17-FL binds to wild-type eIF4E, interestingly, we see a slight decrease in fluorescence intensity of fluorescein (Figure 2.5B). The quenching of the fluorescein dye in the formation of the eIF4E ● mRNA complex could be explained by eIF4E binding to the mRNA. eIF4E, when bound to the mRNA, can change the conformation and result in a slight decrease in intensity. With the formation of the eIF4E-TMR ● S17-FL

complex, however, there is a significant decrease in fluorescence intensity, relative to the S17-FL and eIF4E ● S17-FL intensities (Figure 2.5B). This observation is similar to what we see in our gel-shift assay (Figure 2.5A). While we do see a slight increase in fluorescence intensity at 570 nM, the emission wavelength of TMR, it is not clear that it could be a result of FRET. FRET is a sensitive technique that is not only dependent on distance; other factors include the lifetime of the fluorescent dyes, the positioning of the donor and acceptor dyes, etc[62,63]. However, we still demonstrate with a shorter mRNA that eIF4E-TMR quenches the 3' dye on S17. On the other hand, fluorescence quenching with a longer mRNA does not occur.

While S17-FL bound to eIF4E-TMR shows significant quenching, a longer mRNA bound to eIF4E-TMR does not. CRC1 is a 112-nucleotide mRNA with a 20-nucleotide poly-A tail, derived from the Nanoluciferase mRNA. When eIF4E-TMR is bound to CRC1, we observe a shift, indicating the formation of the eIF4E-TMR ● CRC1-FL complex. Because CRC1 is a larger mRNA than S17, the protein-mRNA migrates further because of the more negatively charged mRNA. This can be seen in the TMR scan visualizing eIF4E-TMR (Figure 2.5). With an excess amount of eIF4E, a portion of the protein shifts downwards, indicating the protein-mRNA complex (Figure 2.5A). As shown in lane six, the eIF4E-TMR ● CRC1-FL migrates further than the eIF4E-TMR ● S17-FL complex (Figure 2.5A). A composite scan shows the overlap of the two scans, and we can see the mRNA-protein complex overlapping from the fluorescein and TMR scans (Figure 2.5A). Interestingly, the eIF4E-TMR ● CRC1-FL complex has similar intensity to the eIF4E ● CRC1-FL complex, unlike the protein-mRNA complex containing S17-FL. In addition, the fluorescence emission scan shows that eIF4E-TMR

does not provide any additional quenching of the mRNA compared to wild-type unlabeled eIF4E. CRC1 is a 112-nucleotide mRNA, significantly longer than the 18-nucleotide S17. Because eIF4E binds to the 5’ cap, eIF4E-TMR may not be able to quench the 3’ end of a longer mRNA strand. Therefore, we have shown a distance-dependent quenching of the fluorescent dye on mRNA when bound to eIF4E-TMR. Using this to our advantage, we wanted to assemble the mRNA-closed loop model to see if we could monitor the 5’ and 3’ proximity.

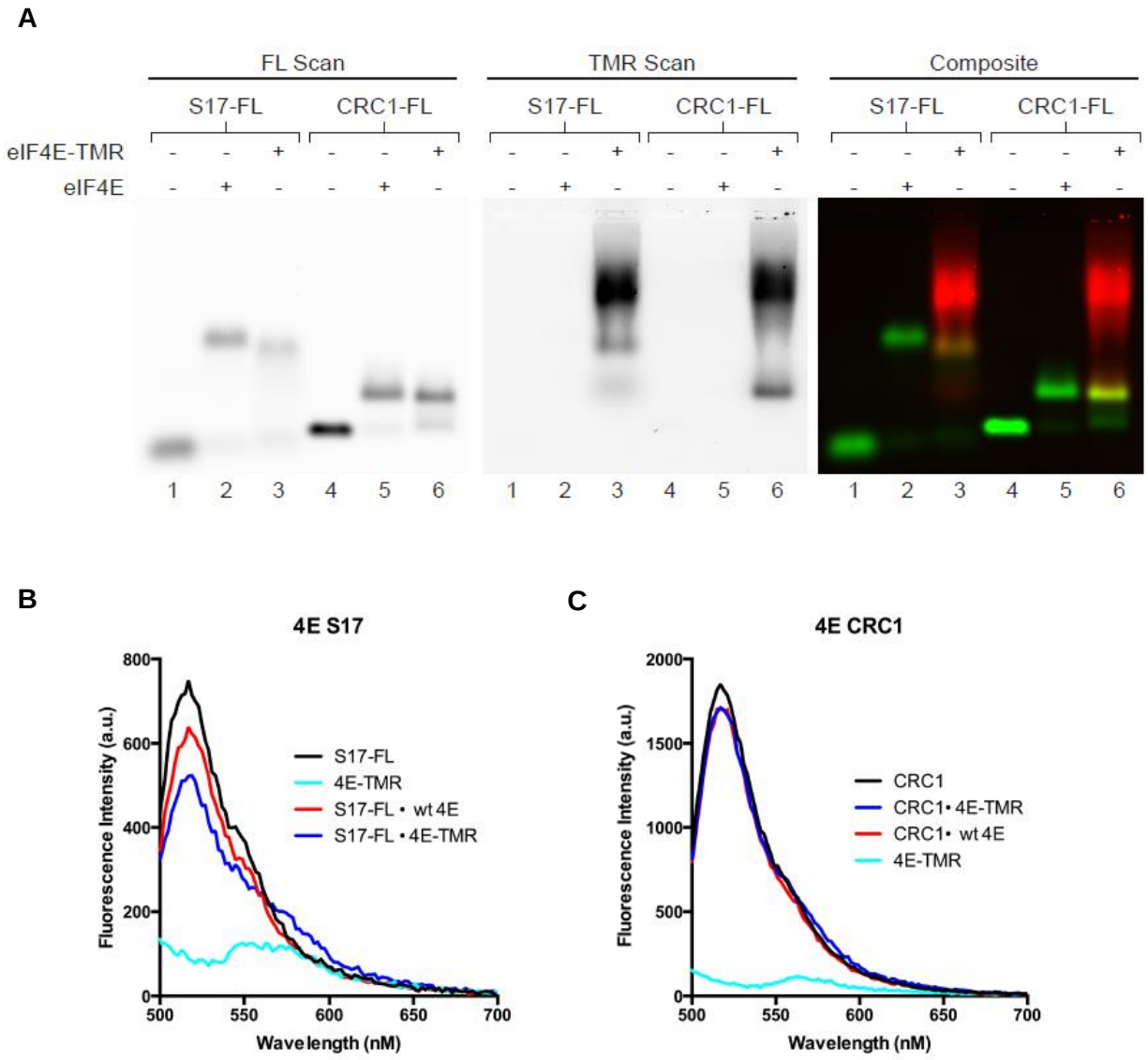

Figure 2.5 Short mRNA's exhibit quenching when bound to eIF4E-TMR, but long mRNA's do not. (A) A gel-shift assays with both CRC1-FL and S17-FL mRNA's bound to wild-type eIF4E and eIF4E-TMR. A concentration of 50 nM and 500 nM were used to the mRNA's and proteins, respectively. First two scans are visualizing the separate fluorescent dyes, and third scan is a composite made in FIJI. (B) Fluorescent emission scan of fluorescein with S17-FL. A 5 nM mRNA concentration was used, and 50 nM concentration of protein. (C) Fluorescent emission scan of fluorescein with CRC1-FL. A 10 nM mRNA concentration is used, and 100 nM concentration of protein.

2.6: Assembling the Closed-loop mRNA model

After establishing eIF4E-TMR's functionality, we wanted to assemble the closed-loop mRNA complex. The closed-loop mRNA model composes of eIF4E, eIF4G, PABP, and capped and tailed mRNA[40] eIF4E binds the 5' cap as PABP binds the 3' poly-A tail, while eIF4G binds both eIF4E and PABP, bringing the 5' and 3' ends into proximity. Based on our previous experiments, we have demonstrated eIF4E-TMR can be used as a tool to monitor the proximity of the 5' and 3' end of the mRNA. Therefore, we hypothesize that if the closed-loop model brings the 5' and 3' ends into proximity, fluorescent quenching of the 3' mRNA fluorophore may be possible. Additionally, FRET may also be possible when the complex assembles. Since we have shown that eIF4E-TMR does not quench CRC1-FL, we decided to use this mRNA in the assembly of our closed-loop mRNA complex.

Using both eIF4E-TMR and CRC1-FL on a gel-shift assay, we observe different migration patterns with the addition of each protein. Figure 3.1 shows the possible protein-mRNA complexes before completely assembling the mRNA ● eIF4E ● eIF4G ● PABP complex. Utilizing the FL label on the mRNA, we can track the migration of the mRNA scanning for FL. In lane 1, we see that eIF4E-TMR binds to CRC1 (Figure 2.7A). No quenching is observed, since the 3' end is not within proximity of eIF4E. Because eIF4G 88-653 does not contain an RNA binding domain, no shift is observed (Lane 3, Figure 2.7A). On the other hand, with the addition of PABP, we observe the formation of the mRNA ● PABP complex, where PABP binds to the poly-A tail. Now that we established the interactions of each protein with the mRNA, we wanted to assemble the other possible mRNA-protein complexes.

In lane 5, we see a super-shift of the CRC1 ● eIF4G ● eIF4E-TMR complex. The complex formed currently has the proteins positioned at the 5’ cap, as seen in figure 3.1. Next, lane 6 contains the CRC1 ● PABP ● eIF4E-TMR complex, where a slight shift is observed relative to lane 4. In this complex, the eIF4E is bound to the 5’ cap, and PABP is bound to the opposite 3’ end (Figure 3.1). Lane 7 contains the CRC1 ● PABP ● eIF4G complex. We observe a super-shift, a result of eIF4G binding to PABP.

Finally, in lane 8 we have the assembly of all the proteins. Interestingly, the complex migrates further than the CRC1 ● PABP ● eIF4G complex. Our previous gel-assays show that the addition of proteins cause the mRNA band to migrate slower. However, size is not the only determinant of how the complex migrates – it can also be determined by the complex’s 3-dimensional shape or charge[64]. When the mRNA closed-loop complex is assembled with eIF4E, its overall charge may become more negatively charged, causing it to migrate more. In addition, the mRNA-closed loop complex may be more compact than the CRC1 ● PABP ● eIF4G complex, which could suggest the formation of the closed loop mRNA (Figure 2.6).

The TMR labeled eIF4E allows us to visualize the protein interactions through eIF4E by scanning for TMR. Not only can we see the formation of the eIF4E ● CRC1 complex, but we can also see excess, unbound eIF4E indicated by the top, smeared band (Lane 2, Figure 2.7A). Lane 5 contains the eIF4E ● eIF4G ● mRNA complex, indicated by the shift and smear downwards. Interestingly, we can also observe the formation of eIF4E ● eIF4G complex, indicated by the sharp band that is shifted upwards relative to free eIF4E in lane 2 (Figure 2.7A). Lane 6 contains the eIF4E ● PABP ● mRNA complex, indicated by the sharp band. While PABP does not directly

bind to eIF4E, both proteins bind to the opposite ends of the mRNA, resulting in a slight upwards shift relative to the band in lane 6. Finally, we see the assembly of the entire complex in lane 8, forming a solid band with no apparent smearing. The migration of this final complex is different from the migration of the other protein complexes, suggesting the formation of the mRNA ● eIF4E ● eIF4G ● PABP complex (Figure 2.7A). Since eIF4E appears to migrate in the same area of the complex, we overlapped the two fluorescent scans to confirm the colocalization of the bands.

Because both images are scanned in the same position, we can overlap them and determine the comigration of different proteins and mRNA. One example is lane 6, which contains both eIF4E-TMR and CRC1-FL. By overlapping both the FL and TMR scans, we observe that the bands co-migrate, indicated by the orange-colored band (Figure 2.7A). In addition, we used FIJI to quantify and plot the FL and TMR intensity of each lane. In figure 2.7B, we see that in lane six the plot peaks overlap perfectly. Therefore, we can be confident that the bands are comigrating and forming the mRNA ● eIF4E ● PABP complex. In lane 5, the large red peak represents the eIF4E ● eIF4G protein complex. A small green peak is seen overlapping the large red peak; this indicates the mRNA ● eIF4E ● eIF4G complex. Finally, we can use this to look at the formation of the CRC1 ● PABP ● eIF4G ● eIF4E complex. The red and green peak corresponding to each band from TMR and FL overlap in lane 8's fluorescence quantification, suggesting that the proteins and mRNA are forming the complex that we expect. Using eIF4E-TMR allows us to visualize the CRC1 ● PABP ● eIF4G ● eIF4E complex through a protein instead of an mRNA and can provide us with additional evidence of the complex formation.

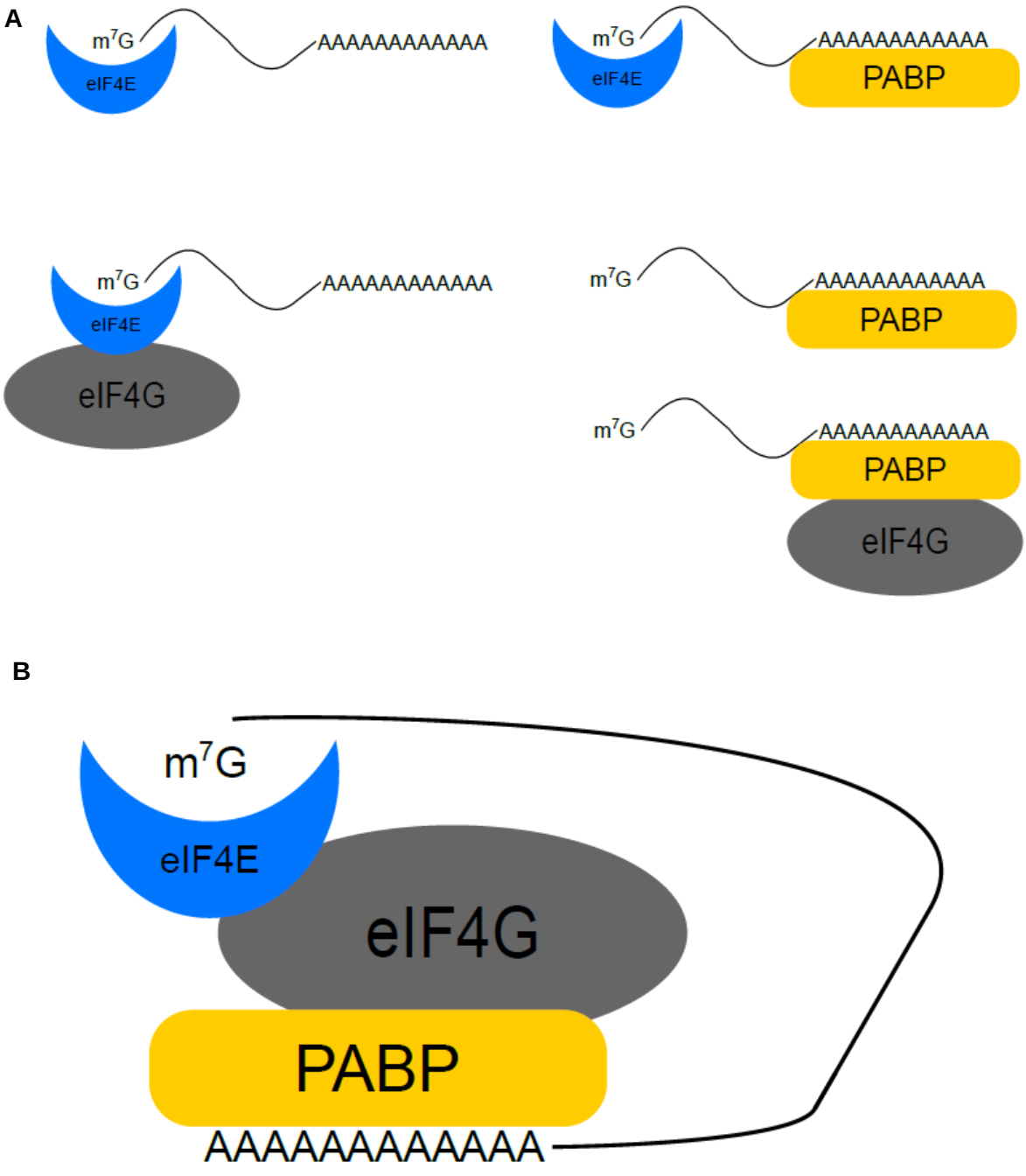

Figure 2.6. Assembly of the Closed-loop mRNA complex. (A) Diagram of the various configurations of protein-mRNA complexes. (B) Assembly of the closed-loop mRNA complex.

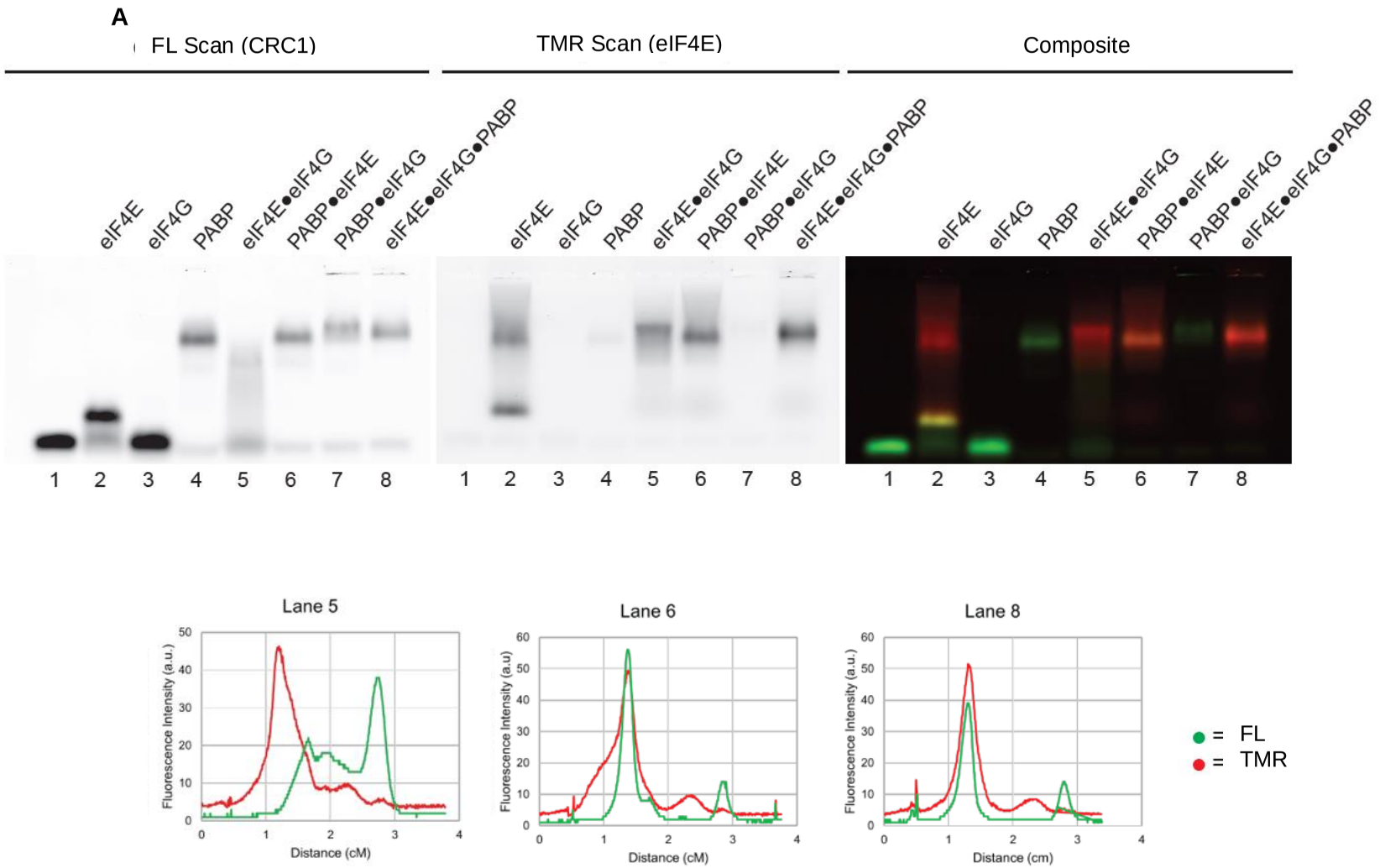

Figure 2.7. Gel-shift assay of mRNA closed-loop complex. (A) Gel-shift assay assembling the closed-loop mRNA model, shown in FL, TMR, and Composite. mRNA concentration used was 50 nM, eIF4E concentration was 250 nM, and eIF4G and PABP had a concentration of 500 nM. (B) Measurement of fluorescence intensity across each lane. Calculations were made through FIJI

2.7: Fluorescence Change of protein-mRNA complexes

Now that we established the formation of the different mRNA-protein complexes in gel, we wanted to see if we would observe FRET when assembling the closed-loop complex. In the fluorescent emission scan, we are monitoring the fluorescein label on the 3' end of the mRNA. Therefore, when we assemble the mRNA closed-loop model, we hope to see FRET to indicate the 5' – 3' proximity. When eIF4E-TMR is bound to CRC1, we see a slight decrease in fluorescence intensity (Figure 2.8). We theorize this decrease resulted from a conformational change when eIF4E binds to the mRNA, as shown in our previous experiments (Figure 2.5C). Interestingly, when we add PABP and form the mRNA ● eIF4E ● PABP complex, we observe a significant decrease in fluorescence intensity. Because our fluorescein dye is located on the 3' end, we believe PABP could quench the emission of the dye when binding to the 3' poly-A tail.

Finally, in the mRNA ● eIF4E ● PABP ● eIF4G complex, we observe a further decrease in fluorescence intensity. This could be due to a multitude of reasons: eIF4G binding to eIF4E, eIF4G binding to PABP, or eIF4G binding to both PABP and eIF4E. In addition, this also could also be a result of eIF4E-TMR quenching the fluorescein dye, confirming the 5' – 3' proximity and the formation of the closed-loop structure. However, we do not observe FRET. FRET is not only dependent on distance, but also the FRET pairs and positioning of the dyes[61-63]; FL and TMR maybe not be the best FRET pairs in this situation. Regardless, this provides promising evidence that we observed the formation of the closed-loop model. However, more studies will need to be done to validate this observation.

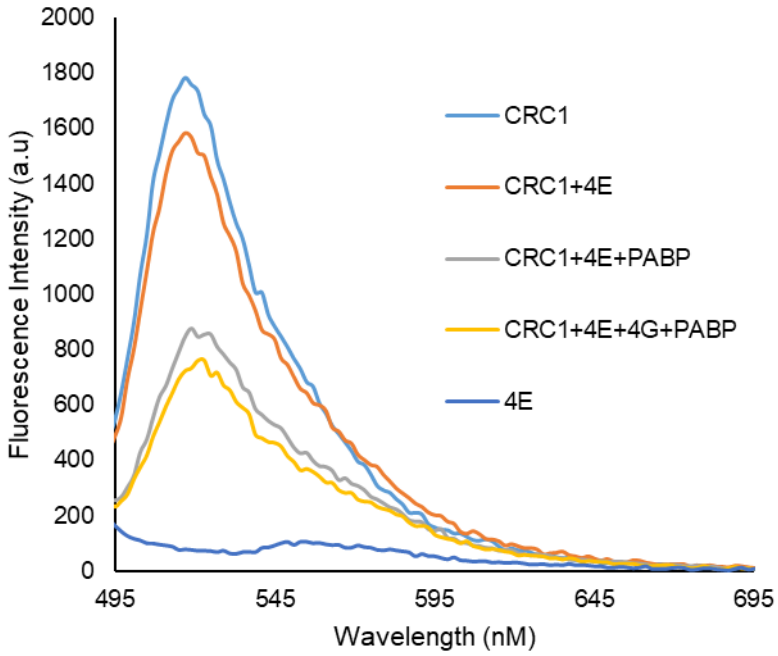

Figure 2.8. Fluorescent intensities of each complex formation. Reactions were run on a Tecan Spark, excited at a wavelength of 465 nM. Emission scan is read from 495 to 700 nM.

Chapter 3: Conclusions and Future Directions

Our original goal of fluorescently labeling eIF4E was to create single-cysteine constructs of the protein. However, we have shown that mutating the cysteine residues significantly impairs eIF4E's ability to bind to the 5' cap of mRNA. Although the crystal structure does not predict eIF4E has disulfide bonds, there may indeed be disulfide bridge formations. Mutating the cysteines seems to disrupt the integrity of the structure of eIF4E, leading to poor binding of the 5' cap. Interestingly, we observe that eIF4G rescues the binding affinity of eIF4E to form the eIF4E ● eIF4G ● mRNA complex. eIF4G seems to enhance the affinity of eIF4E to capped mRNA, shown similarly in previous studies.

Because single cysteine mutants of eIF4E were not very active in binding to the capped mRNA, we had to develop an alternative method of fluorescently labeling eIF4E. Using the sortase enzyme, we successfully labeled eIF4E at the C-terminal end. Our labeled protein, eIF4E-TMR, successfully binds to capped mRNA with similar affinity as wild-type. We have demonstrated that eIF4E-TMR, when bound to the 5' cap, can fluorescently quench the 3' end of a short mRNA. Therefore, we can use this as a method to show the formation of the closed-loop mRNA model where the 5' and 3' ends are in proximity to each other.

Our gel-shift assay shows the assembly of the proteins within the closed-loop complex. Due to the different migration patterns, it suggests we can assemble the mRNA ● eIF4E ● eIF4G ● PABP complex. In solution, the emission peak of the fluorescent mRNA in complex with eIF4E, eIF4G, and PABP is the lowest. This may suggest the formation of the closed-loop model, bringing the 5' and 3' ends into

proximity. However, FRET is not observed, and the quenching can result from various factors other than the 5’ – 3’ proximity. Therefore, much is to be explored within this elusive complex.

3.1: Observe FRET in Assembly of Closed-loop mRNA Complex

When assembling the mRNA closed-loop complex, we observe the quenching of the fluorescent dye on the mRNA. Some conformational change is occurring that decreases the fluorescence intensity. However, we cannot completely attribute this to the 5’ end approaching the proximity of the 3’ end. Therefore, to provide more evidence that the “closed loop” is forming, we hope to see FRET. We want to explore other well-known FRET pairs such as Cy3 and Cy5 dyes. Hopefully, with these dyes, we can see FRET and confidently confirm the formation of the mRNA closed-loop structure.

3.2: Study the Dynamics of the mRNA Closed-loop complex

Little is still known about the eIF4E ● eIF4G ● PABP ● mRNA complex – is it an extremely stable complex, or is it extremely dynamic, constantly changing? It would be interesting to study how eIF4E, the rate-limiting protein for translation, dissociates and is reused to reinitiate translation. We hope to label the other proteins with a fluorescent dye and study the different protein-mRNA complexes. This way, we can determine the binding constants of each complex, and understand more about the stability of this essential complex. In addition, we want to solve the structure using Cryo-EM.

3.3: Purify Full length eIF4G

We have successfully purified each full-length protein used in our binding studies. However, the purification of full-length eIF4G still remains challenging. Because it is such an intrinsically disordered protein, currently only shorter fragments are viable. While these fragments are great in binding studies, only the full-length protein will truly show the natural dynamics of these protein interactions. Therefore, we want to purify the full-length eIF4G. We hope with this full-length protein, we can uncover more about the mechanism of translation initiation.

3.4: Investigate eIF4E with well-known binding partners

With eIF4E labeled with a fluorescent dye, it opens avenues to visualize the interactions of eIF4E with well-characterized binding partners. One example would be looking at the interactions of eIF4E and 4EBP, a protein that is a powerful regulator of eIF4E.

Chapter 4: Materials and Methods

4.1 Expression and Purification of eIF4E constructs

The eIF4E plasmid was transformed into *E. coli* Rosetta 2 (DE3) pLysS competent cells. 2 5 mL LB starter cultures were made with 100 ug/mL ampicillin and 25 ug/mL chloramphenicol, and grown overnight at 37°C. 2 1 liter LB flasks with 100 ug/mL ampicillin and 25 ug/mL chloramphenicol were inoculated with the starter culture, and grown at 37°C, until the OD_{600} reached approximately 0.5. The culture was cooled to 14°C, induced with 0.2 mM IPTG and grown at the same temperature overnight for 14 – 16 hours. The following day, the cell culture was spun down at 5000 RPM for 15 minutes at 4°C and the pellet was then stored in -80°C.

On the day of purification, the pellet was resuspended in buffer 1 supplemented with PMSF and β-mercaptoethanol (100 mM Tris-HCl pH 8.0, 100 mM KCl, 10% Glycerol, 5 mM Imidazole, 1 mM PMSF, 5 mM β-mercaptoethanol). The lysate was then lysed with a French press and clarified by spinning at 12.5K RPM for 45 minutes. The clarified lysate was loaded onto a pre-equilibrated column containing Ni-NTA beads at a flow rate of 0.8 mL/min. The column containing the resin was then washed with 20 column volumes of buffer A supplemented with Heparin sodium salt (100 mM Tris-HCl pH 8.0, 100 mM KCl, 10% Glycerol, 5 mM Imidazole, 1 mM PMSF, 5 mM β-mercaptoethanol, 1 mg/mL Heparin sodium salt). Following that, the column was washed with 20 column volumes of a high salt buffer (100 mM Tris-HCl pH 8.0, 1 M KCl, 10% glycerol). Lastly, the column was washed with buffer 2 (100 mM Tris-HCl pH 8.0, 100 mM KCl, 10% glycerol, 20 mM Imidazole). The protein was then eluted in a high

Imidazole buffer (20 mM Tris-HCl pH 8.0, 100 mM KCl, 10% Glycerol, 5 mM β-mercaptoethanol). Eluted fractions were analyzed on an SDS-PAGE gel, and fractions containing protein were concentrated with centrifugal filters (Amicon) until the total volume was ~2 mL.

The concentrated sample was run through a Superdex 200 16/60 gel filtration column (GE) in buffer A (20 mM Tris-HCl, pH 8.0, 100 mM NaCl, 10% glycerol). Fractions containing the protein were further concentrated until the volume was ~3 mL, and loaded onto a Hitrap Q HP 5 mL anion column with Buffer A (20 mM Tris-HCl, pH 8.0, 100 mM NaCl, 10% glycerol), and Buffer B (20 mM Tris-HCl, pH 8.0, 1 M NaCl, 10% glycerol) at a target gradient of 50% B in 20 CV. Fractions containing the protein were concentrated, flash-frozen, and stored in -80°C.

4.2 Expression and Purification of Poly-A Binding Protein (PABP)

Human PABP in the pANT7_cGST vector was subcloned into pMCSG26. Afterwards, the pMCSG26 plasmid containing PABP was transformed into *e. coli* Rosetta 2 pLysS cells. 4 5 mL starter cultures were grown at 37°C overnight, and were used to inoculate 4 1 L flasks supplemented with 100 ug/mL ampicillin and 25 ug/mL chloramphenicol. The cultures were grown at 37°C and were induced with 0.25 mM IPTG when the OD of the cultures reached approximately 0.5. They were then grown overnight for 12-16 hours at 18°C. The following day, the cell culture was spun down at 5000 RPM for 15 minutes at 4°C and the pellet was then stored in -80°C.

On the day of purification, the pellet was resuspended in 50 mL of Lysis buffer (25 mM Tris, pH 7.5, 500 mM NaCl, 0.5 mM EDTA, 5 mM Imidazole, 8 mM DTT, 0.5

mM PMSF, 0.1% Triton-X 100, 5% Glycerol). Lysate was then pulse-sonicated and clarified by spinning down for 12.5K rpm for 45 minutes. Once clarified, the lysate was loaded onto a column containing pre-equilibrated Ni-NTA beads at a flow rate of 0.8 mL/minute. The column was then washed with 25 column volumes of wash buffer (25 mM Tris, pH 7.5, 500 mM NaCl, 0.5 mM EDTA, 20 mM Imidazole, 8 mM DTT, 5% Glycerol).

The protein was then eluted in elution buffer (25 mM Tris, pH 7.5, 500 mM NaCl, 0.5 mM EDTA, 50 mM Imidazole, 8 mM DTT, 5% Glycerol), and the fractions were concentrated to about 1 mL. The concentration elution was then run through a Hitrap Heparin HP column, with buffer A (25 mM Tris-HCl, pH 7.5, 0.5 mM TCEP-HCl, 5% Glycerol), and buffer B (25 mM Tris-HCl, pH 7.5, 0.5 mM TCEP-HCl, 1 M NaCl, 5% Glycerol) at a target gradient of 100% B over 30 CV. Fractions corresponding to the protein were ran on an SDS-PAGE to confirm, and further concentrated to 1 mL and ran through the Superdex 200 16/60 column, containing buffer (25 mM Tris-HCl, pH 7.5, 250 mM NaCl, 0.5 mM TCEP-HCl, 5% Glycerol). Fractions containing the protein were concentrated, flash frozen and stored at -80°C.

4.3 Expression and Purification of eIF4G1 constructs

Two eIF4G1 constructs were primarily used in the binding studies: eIF4G 88-653 and MBP eIF4G 565-653. The human eIF4G isoform 5 was codon-optimized for *E. coli* expression and purchased from Genewiz. eIF4G 88-653 was cloned into the pTXB1 vector, which contains a C-terminal Mxe intein/chitin binding domain, helpful for

purification purposes. eIF4G 565-653 was cloned in the pMCSG9 vector, which contains an N-terminal Maltose binding protein (MBP) tag for high yields in purification.

Both plasmids with the two protein constructs were transformed into BL21* *e. coli* cells. 5 mL starter cultures that were grown overnight at 37°C were used to inoculate 1 L flasks containing LB, supplemented with 100 ug/mL ampicillin. The cultures continued to grow at 37°C, and were induced with 0.4 mM IPTG once the OD reached ~0.5. Cell cultures were cooled to 30°C, and grew for 2.5-3 hours. Cell cultures were spun down at 5K rpm for 15 minutes, and the pellets were stored in the -80°C until further use.

Cells expressing MBP eIF4G 565-653 were resuspended in lysis buffer (50 mM Tris-HCl, pH 8.0, 600 mM NaCl, 10 mM Imidazole, 0.5% Triton X-100, 1mM PMSF, 10% Glycerol), and pulse-sonicated and clarified at 12.5K RPM for 45 minutes. Clarified lysate was poured into a pre-equilibrated column containing Ni-NTA beads, allowing a flow of 0.8 mL/minute. Column was then washed with wash buffer 1 (50 mM Tris-HCl, pH 8.0, 1 M NaCl, 20 mM Imidazole, 0.5% Triton X-100, 1 mg/mL Heparin sodium salt, 10% Glycerol). Afterwards, the column was washed with wash buffer 2 (50 mM Tris-HCl, pH 8.0, 100 mM NaCl, 20 mM Imidazole, 10% Glycerol). Finally, the protein was eluted with elution buffer (50 mM Tris-HCl, pH 8.0, 100 mM NaCl, 250 mM Imidazole, 10% Glycerol). Elution fractions were analyzed via SDS-PAGE, and fractions containing protein were concentrated.

Cells expressing eIF4G 88-653 were resuspended in lysis buffer (20 mM HEPES, pH 8.5, 100 mM NaCl, 1 mM PMSF, 10% Glycerol). Cell lysate was then pulse-sonicated, and clarified at 12.5K RPM for 45 minutes. Clarified lysate was then batch-bound with 10 mL of pre-equilibrated Chitin binding beads for 2-3 hours. Lysate

containing Chitin binding beads were poured into a column with a flow rate of 1 ml/minute. Column containing Chitin binding beads were washed with 5 column volumes of wash buffer 1 (20 mM HEPES, pH 8.5, 100 mM NaCl, 1 mg/mL Heparin sodium salt, 10% Glycerol). Column was then washed with 10 column volumes of wash buffer 2 (20 mM HEPES, pH 8.5, 1 M NaCl, 10% Glycerol). Lastly, column was washed with 5 column volumes of wash buffer 3 (20 mM HEPES, pH 8.5, 100 mM NaCl, 10% Glycerol). Elution buffer (20 mM HEPES, pH 8.5, 100 mM NaCl, 50 mM DTT, 10% Glycerol) was added to the column and incubated overnight. The following day, elutions were collected, and fractions were analyzed via SDS-PAGE, where fractions containing protein were concentrated.

Both protein construct elutions were ran through the Superdex 200 16/60, containing 4F buffer (20 mM Tris-HCl, pH 8.0, 100 mM KCl, 10% Glycerol). Fractions containing the proteins were concentrated, flash-frozen and stored at -80°C.

4.4 Electrophoretic Mobility Shift Assay

Reactions were incubated with binding buffer (50 mM Tris pH 8.0, 150 mM KCl, 1 mM DTT, 0.01% Tween20, 50 ng/µl total tRNA from E. coli) for a total of 1 hour at room temperature. Before loading, 50% prechilled Glycerol was added to the mixture. Gels were run on a 0.6% Seakem GTG agarose at 4°C in 1X TBE buffer, surrounded by ice. Gels were run at 66V for 75 minutes, and were visualized either on a Typhoon FLA9500 or Amersham Typhoon.

4.5 In Vitro Transcription of RNA

The DNA template of the RNA was incubated for 2 hours with 5 mM DTT, 4 mM AUGC (NTP mix), T7 RNA polymerase, and 1X Trx Buffer (40 mM Tris-HCl, pH 8.0, 20 mM $MgCl_2$, 2 mM Spermidine, 0.1% Triton-X 100). A series of chloroform extractions were performed, and the RNA sample was loaded onto a pre-run 1.5 mm thick 8% denaturing polyacrylamide gel with 2X loading dye (95% formamide, 20 mM EDTA, 0.05% xylene cyanol and 0.05% bromophenol blue). The gel was run in 1X TBE buffer at room temperature for approximately 2.5 hours at 30 watts. The RNA band was visualized through UV shadowing, and a clean, sharp razor was used to excise the RNA band from the gel. The RNA band was then incubated with RNA elution buffer (0.5 M sodium acetate pH 5.2, 0.1 mM EDTA pH 8.0, 0.1% SDS) at 4°C, constantly rotating. The following day, a total of 3 chloroform extractions were performed, along with an ethanol precipitation. The RNA pellet was resuspended in MQ water, and stored at -80°C until further use.

4.6 5’ Capping Reaction of RNA

Approximately 300 pmoles of RNA was incubated at 65°C for 5 minutes, then on ice for 5 minutes. Afterwards, the RNA was incubated at 37°C for 2 hours in the following conditions: 1X Capping Buffer (50 mM Tris-HCl pH 8.0, 5 mM KCl, 1 mM $MgCl_2$), 0.5 mM GTP, 0.1 mM S-adenosylmethionine (SAM), and Vaccinia capping enzyme. RNA then was purified through the Monarch RNA cleanup kit. Capped RNA was stored at -80°C until further use.

4.7 3’ Labeling of RNA with fluorescein 5-thiosemicarbizide

0.5 nmoles of RNA was oxidized for 90 minutes at room temperature in 100 mM sodium acetate pH 5.2, 100 uM KIO_4. RNA was then purified through a Monarch RNA cleanup kit and incubated with fluorescein 5-thiosemicarbizide (1.5 mM fluorescein, 100 mM sodium acetate pH 5.2). Reaction was incubated overnight in the 4°C. The following day, labeled RNA was further purified through a Monarch RNA cleanup kit, and stored at -80°C.

4.8 Fluorescent Anisotropy Binding Assay

Reactions were incubated with binding buffer (50 mM Tris pH 8.0, 150 mM KCl, 1 mM DTT, 0.01% Tween20, 50 ng/µl total tRNA from E. coli) for a total of 1 hour at room temperature. Samples were loaded onto a Greiner Black 384 well plate, and the anisotropy measurements were read by a Tecan Spark. An excitation wavelength of 490, and a polarized emission of 520 were used from the prebuilt filters. The G-factor was previously determined by a control sample of fluorescein. The anisotropy values were exported to Graphpad Prism, where the K_d value can be determined using the following equation,

$$\frac{[\mathrm{P}+\mathrm{L}]}{[\mathrm{L}]} = \frac{[[\mathrm{P}]+[\mathrm{L}]+\mathrm{K_D}-\sqrt{([\mathrm{P}]+[\mathrm{L}]+\mathrm{K_D})^2-4[\mathrm{P}][\mathrm{L}]}}{(2[\mathrm{P}])}$$

where [P+L]/[L] is the anisotropy value, [L] is the ligand, and [P] is the protein concentration.

4.9 Fluorescein Emission Scan Assay

Reactions were incubated with binding buffer (50 mM Tris pH 8.0, 150 mM KCl, 1 mM DTT, 0.01% Tween20, 50 ng/µl total tRNA from E. coli) for a total of 1 hour at room temperature. Samples were loaded onto a Greiner Black 384 well plate, and were excited at 465 nM with a bandwidth of 10 nM, and fluorescein emission was read from 495 nM to 700 nM.

4.10 Labeling GGGGC peptide with Tetramethylrhodamine

A lyophilized oligopeptide (GGGGC) purchased from Bon Opus Biosciences was resuspended in 1X PBS buffer. A 1:2 molar ratio of the peptide and tetramethylrhodamine (TRITC) was incubated overnight in 4°C with a molar excess of TCEP to reduce and prevent disulfide bridges. The following day, the maleimide labeled peptide was ran through a Vydac C18 250x10mm 5µm column with a percent gradient of 5% to 80% over 40 minutes, with buffer A containing MQ water with 0.1% trifluoroacetic acid, and buffer B containing acetonitrile with 0.1% trifluoroacetic acid. The peak corresponding to the labeled peptide was then lyophilized in the Speedvac, resuspended in DMSO, and stored in -80°C until further use.

4.11 Sortase labeling reaction of eIF4E

eIF4E containing the sortase motif was incubated with the sortase enzyme at room temperature under the following conditions: 50 mM Tris-HCl, pH 7.5. 150 mM NaCl, 10 mM $CaCl_2$, 50 uM eIF4E, 1mM peptide, 2.5 uM sortase. In order to remove

excess labeled peptide, the solution was dialyzed using Slide-A-Lyzer Dialysis Cassettes (Thermofisher). Afterwards, a small amount of Ni-NTA beads were added to the solution to bind the sortase enzyme and any unlabeled protein. Spin-X columns were then used to remove the Ni-NTA beads containing sortase and unlabeled protein. Clean, labeled protein was then flash-frozen and stored at -80°C.

References

1. Pestova, T. V., Kolupaeva, V. G., Lomakin, I. B., Pilipenko, E. V., Shatsky, I. N., Agol, V. I., & Hellen, C. U. (2001). Molecular mechanisms of translation initiation in eukaryotes. Proceedings of the National Academy of Sciences, 98(13), 7029-7036.

2. Bednarek, S., Madan, V., Sikorski, P.J., Bartenschlager, R., Kowalska, J. and Jemielity, J., 2018. mRNAs biotinylated within the 5′ cap and protected against decapping: new tools to capture RNA–protein complexes. Philosophical Transactions of the Royal Society B: Biological Sciences, 373(1762), p.20180167.

3. Hashem, Y., & Frank, J. (2018). The jigsaw puzzle of mRNA translation initiation in eukaryotes: a decade of structures unraveling the mechanics of the process. Annual review of biophysics, 47, 125-151.

4. Shatsky, I. N., Terenin, I. M., Smirnova, V. V., & Andreev, D. E. (2018). Cap-independent translation: What's in a name?. Trends in biochemical sciences, 43(11), 882-895.

5. Svitkin, Y. V., Pause, A., Haghighat, A., Pyronnet, S., Witherell, G., Belsham, G. J., & Sonenberg, N. (2001). The requirement for eukaryotic initiation factor 4A (eIF4A) in translation is in direct proportion to the degree of mRNA 5'secondary structure. Rna, 7(3), 382-394.

6. Jankowsky, E., Gross, C. H., Shuman, S., & Pyle, A. M. (2001). Active disruption of an RNA-protein interaction by a DExH/D RNA helicase. Science, 291(5501), 121-125.

7. Jossé, L., Xie, J., Proud, C. G., & Smales, C. M. (2016). mTORC1 signaling and eIF4E/4E-BP1 translation initiation factor stoichiometry influence recombinant protein productivity from GS-CHOK1 cells. Biochemical Journal, 473(24), 4651-4664.

8. Peter, D., Igreja, C., Weber, R., Wohlbold, L., Weiler, C., Ebertsch, L., Weichenrieder, O., & Izaurralde, E. (2015). Molecular Architecture of 4E-BP Translational Inhibitors Bound to eIF4E. *Molecular Cell*, *57*(6), 1074–1087. https://doi.org/10.1016/j.molcel.2015.01.017

9. Mader, S., Lee, H., Pause, A., & Sonenberg, N. (1995). The Translation Initiation Factor eIF-4E Binds to a Common Motif Shared by the Translation Factor eIF-4 and the Translational Repressors 4E-Binding Proteins. Molecular and Cellular biology (Vol. 15, Issue 9).

10. Rosenwald, I. B., Chen, J.-J., Wang, S., Savas, L., London, I. M., & Pullman, J. (1999). Upregulation of protein synthesis initiation factor eIF-4E is an early event during colon carcinogenesis. *Oncogene*, *18*(15), 2507–2517.

11. Wang, R., Geng, J., Wang, J. hua, Chu, X. yuan, Geng, H. cheng, & Chen, L. bang. (2009). Overexpression of eukaryotic initiation factor 4E (eIF4E) and its clinical significance in lung adenocarcinoma. *Lung Cancer*, *66*(2), 237–244.

12. Salehi, Z., Mashayekhi, F., & Shahosseini, F. (2007). Significance of eIF4E expression in skin squamous cell carcinoma. *Cell Biology International*, *31*(11), 1400–1404.

13. Holm, N., Byrnes, K., Johnson, L., Abreo, F., Sehon, K., Alley, J., Meschonat, C., Md, Q. C., & Li, B. D. L. (2008). A prospective trial on initiation factor 4E (eIF4E) overexpression and cancer recurrence in node-negative breast cancer. *Annals of Surgical Oncology*, *15*(11), 3207–3215.

14. Robichaud, N., del Rincon, S. v., Huor, B., Alain, T., Petruccelli, L. A., Hearnden, J., Goncalves, C., Grotegut, S., Spruck, C. H., Furic, L., Larsson, O., Muller, W. J., Miller, W. H., & Sonenberg, N. (2014). Phosphorylation of eIF4E promotes EMT and metastasis via translational control of SNAIL and MMP-3. *Oncogene*, *34*(16), 2032–2042.

15. Walsh, D., & Mohr, I. (2004). Phosphorylation of eIF4E by Mnk-1 enhances HSV-1 translation and replication in quiescent cells. *Genes and Development*, *18*(6), 660–672.

16. Furic, L., Rong, L., Larsson, O., Koumakpayi, I. H., Yoshida, K., Brueschke, A., Petroulakis, E., Robichaud, N., Pollak, M., Gabouryd, L. A., Pandolfi, P. P., Saad, F., & Sonenberg, N. (2010). EIF4E phosphorylation promotes tumorigenesis and is associated with prostate cancer progression. *Proceedings of the National Academy of Sciences of the United States of America*, *107*(32), 14134–14139.

17. Schü, P., Bumann, M., Oberholzer, A. E., Bieniossek, C., Trachsel, H., Altmann, M., & Baumann, U. (2008). *Crystal structure of the yeast eIF4A-eIF4G complex: An RNA-helicase controlled by protein-protein interactions*.

18. Imataka, H., & Sonenberg, N. (1997). Human Eukaryotic Translation Initiation Factor 4G (eIF4G) Possesses Two Separate and Independent Binding Sites for eIF4A. In *MOLECULAR AND CELLULAR BIOLOGY* (Vol. 17, Issue 12).

19. Korneeva, N. L., Lamphear, B. J., Hennigan, F. L. C., Merrick, W. C., & Rhoads, R. E. (2001). Characterization of the Two eIF4A-binding Sites on Human eIF4G-1. *Journal of Biological Chemistry*, *276*(4), 2872–2879.

20. Lefebvre, A. K., Korneeva, N. L., Trutschl, M., Cvek, U., Duzan, R. D., || C. A. B., || J. W. B. H., & Rhoads, R. E. (2006). Translation Initiation Factor eIF4G-1 Binds to eIF3 through the eIF3e Subunit * NIH Public Access. In *J Biol Chem* (Vol. 281, Issue 32).

21. Goyer, C., Altmann, M., Lee,', H. S., Blanc,' Mohanish Deshmukh, A., Woolford, J. L., Trachsel, H., & Sonenbergl, N. (1993). TIF4631 and TIF4632: Two Yeast Genes Encoding the High-Molecular-Weight Subunits of the Cap-Binding Protein Complex (Eukaryotic Initiation Factor 4F) Contain an RNA Recognition Motif-Like Sequence and Carry Out an Essential Function. In *MOLECULAR AND CELLULAR BIOLOGY*.

22. Yan, R., Rychlik, W., Etchison, D., & Rhoads, R. E. (1992). Amino acid sequence of the human protein synthesis initiation factor eIF- 4γ. *Journal of Biological Chemistry*, *267*(32), 23226–23231.

23. Imataka, H., Gradi, A., & Sonenberg, N. (1998). A newly identified N-terminal amino acid sequence of human eIF4G binds poly(A)-binding protein and functions in poly(A)-dependent translation. In The EMBO Journal (Vol. 17, Issue 24).

24. Park, E. H., Walker, S. E., Lee, J. M., Rothenburg, S., Lorsch, J. R., & Hinnebusch, A. G. (2011). Multiple elements in the eIF4G1 N-terminus promote assembly of eIF4G1•PABP mRNPs in vivo. *EMBO Journal*, *30*(2), 302–316.

25. Tarun, S. Z., & Sachs1, A. B. (1996). Association of the yeast poly(A) tail binding protein with translation initiation factor eIF-4G. In *The EMBO Journal* (Vol. 15, Issue 24).

26. von der Haar, T., Ball, P. D., & McCarthy, J. E. G. (2000). Stabilization of Eukaryotic Initiation Factor 4E Binding to the mRNA 5′-Cap by Domains of eIF4G. Journal of Biological Chemistry, 275(39), 30551–30555.

27. Haghighat, A., & Sonenberg, N. (1997). eIF4g dramatically enhances the binding of eIF4E to the mRNA 5'-cap structure. Journal of Biological Chemistry, 272(35), 21677–21680.

28. Santini, E., Huynh, T. N., Longo, F., Koo, S. Y., Mojica, E., D'Andrea, L., Bagni, C., & Klann, E. (2017). Reducing eIF4E-eIF4G interactions restores the balance between protein synthesis and actin dynamics in fragile X syndrome model mice. *Science Signaling*, *10*(504), 41–46.

29. Pan, X., Yang, X., Zang, J., Zhang, S., Huang, N., Guan, X., Zhang, J., Wang, Z., Li, X., & Lei, X. (2017). Downregulation of eIF4G by microRNA-503

enhances drug sensitivity of MFC-7/ADR cells through suppressing the expression of abc transport proteins. *Oncology Letters*, *13*(6), 4785–4793.

30. Cencic, R., Desforges, M., Hall, D. R., Kozakov, D., Du, Y., Min, J., Dingledine, R., Fu, H., Vajda, S., Talbot, P. J., & Pelletier, J. (2011). Blocking eIF4E-eIF4G Interaction as a Strategy To Impair Coronavirus Replication. *Journal of Virology*, *85*(13), 6381–6389. https://doi.org/10.1128/jvi.00078-11

31. Oberer, M., Marintchev, A., & Wagner, G. (2005). Structural basis for the enhancement of eIF4A helicase activity by eIF4G. *Genes and Development*, *19*(18), 2212–2223.

32. Lomakin, I. B., Hellen, C. U. T., & Pestova, T. v. (2000). Physical Association of Eukaryotic Initiation Factor 4G (eIF4G) with eIF4A Strongly Enhances Binding of eIF4G to the Internal Ribosomal Entry Site of Encephalomyocarditis Virus and Is Required for Internal Initiation of Translation. In *MOLECULAR AND CELLULAR BIOLOGY* (Vol. 20, Issue 16).

33. Kahvejian, A., Svitkin, Y. V., Sukarieh, R., M'Boutchou, M. N., & Sonenberg, N. (2005). Mammalian poly (A)-binding protein is a eukaryotic translation initiation factor, which acts via multiple mechanisms. Genes & development, 19(1), 104-113.

34. Gray, N. K., Coller, J. M., Dickson, K. S., & Wickens, M. (2000). Multiple portions of poly(A)-binding protein stimulate translation in vivo. The EMBO Journal, 19(17), 4723–4733.

35. Grosset, C., Chen, C.-Y. A., Xu, N., Sonenberg, N., Jacquemin-Sablon, H., & Shyu, A.-B. (2000). A Mechanism for Translationally Coupled mRNA Turnover: Interaction between the Poly(A) Tail and a c-fos RNA Coding Determinant via a Protein Complex. In Cell (Vol. 103).

36. de Rozières, C. M., Pequeno, A., Shahabi, S., Lucas, T. M., Godula, K., Ghosh, G., & Joseph, S. (2022). PABP1 Drives the Selective Translation of Influenza A Virus mRNA. Journal of Molecular Biology, 434(5), 167460.

37. Iwakawa, H., Tajima, Y., Taniguchi, T., Kaido, M., Mise, K., Tomari, Y., Taniguchi, H., & Okuno, T. (2012). Poly(A)-Binding Protein Facilitates Translation of an Uncapped/Nonpolyadenylated Viral RNA by Binding to the 3′ Untranslated Region. *Journal of Virology*, *86*(15), 7836–7849.

38. Kahvejian, A., Roy, G., & Sonenberg, N. (2001). The mRNA closed-loop model: The function of PABP and PABP-interacting proteins in mRNA translation. Cold Spring Harbor Symposia on Quantitative Biology, 66, 293–300.

39. Archer, S. K., Shirokikh, N. E., Hallwirth, C. V., Beilharz, T. H., & Preiss, T. (2015). Probing the closed-loop model of mRNA translation in living cells. RNA Biology, 12(3), 248–254.

40. Vicens, Q., Kieft, J. S., & Rissland, O. S. (2018). Revisiting the Closed-Loop Model and the Nature of mRNA 5′–3′ Communication. In Molecular Cell (Vol. 72, Issue 5, pp. 805–812). Cell Press.

41. Wells, S. E., Hillner, P. E., Vale, R. D., & Sachs, A. B. (1998). Circularization of mRNA by Eukaryotic Translation Initiation Factors. Molecular Cell, 2(1), 135–140.

42. Alekhina, O. M., Terenin, I. M., Dmitriev, S. E., & Vassilenko, K. S. (2020). Functional cyclization of eukaryotic mRNAs. International Journal of Molecular Sciences, 21(5).

43. Borman, A. M., Michel, Y. M., & Kean, K. M. (2000). Biochemical characterisation of cap-poly(A) synergy in rabbit reticulocyte lysates: the eIF4G-PABP interaction increases the functional affinity of eIF4E for the capped mRNA 5′-end. In *Nucleic Acids Research* (Vol. 28, Issue 21).

44. Kopeina, G. S., Afonina, Z. A., Gromova, K. V., Shirokov, V. A., Vasiliev, V. D., & Spirin, A. S. (2008). Step-wise formation of eukaryotic double-row polyribosomes and circular translation of polysomal mRNA. *Nucleic Acids Research*, *36*(8), 2476–2488.

45. Afonina, Z. A., Myasnikov, A. G., Shirokov, V. A., Klaholz, B. P., & Spirin, A. S. (2014). Formation of circular polyribosomes on eukaryotic mRNA without cap-structure and poly(A)-tail: A cryo electron tomography study. *Nucleic Acids Research*, *42*(14), 9461–9469.

46. Lai, W. J. C., Kayedkhordeh, M., Cornell, E. V., Farah, E., Bellaousov, S., Rietmeijer, R., Salsi, E., Mathews, D. H., & Ermolenko, D. N. (2018). mRNAs and lncRNAs intrinsically form secondary structures with short end-to-end distances. *Nature Communications*, *9*(1).

47. Leija-Martínez, N., Casas-Flores, S., Cadena-Nava, R. D., Roca, J. A., Mendez-Cabañas, J. A., Gomez, E., & Ruiz-Garcia, J. (2014). The separation between the 5'-3' ends in long RNA molecules is short and nearly constant. *Nucleic Acids Research*, *42*(22), 13963–13968.

48. Pelletier, J., Graff, J., Ruggero, D., & Sonenberg, N. (2015). Targeting the eIF4F Translation Initiation Complex: A Critical Nexus for Cancer Development. *Cancer Research*, *75*(2), 250–263.

49. Toseland, C. P. (2013). Fluorescent labeling and modification of proteins. In Journal of Chemical Biology (Vol. 6, Issue 3, pp. 85–95).

50. Pagano, J. M., Clingman, C. C., & Ryder, S. P. (2011). Quantitative approaches to monitor protein-nucleic acid interactions using fluorescent probes. Rna, 17(1), 14–20.

51. Niedzwiecka, A., Marcotrigiano, J., Stepinski, J., Jankowska-Anyszka, M., Wyslouch-Cieszynska, A., Dadlez, M., Gingras, A. C., Mak, P., Darzynkiewicz, E., Sonenberg, N., Burley, S. K., & Stolarski, R. (2002). Biophysical studies of eIF4E cap-binding protein: Recognition of mRNA 5′ cap structure and synthetic fragments of eIF4G and 4E-BP1 proteins. Journal of Molecular Biology, 319(3), 615–635.

52. Scheper, G. C., Van Kollenburg, B., Hu, J., Luo, Y., Goss, D. J., & Proud, C. G. (2002). Phosphorylation of eukaryotic initiation factor 4E markedly reduces its affinity for capped mRNA. Journal of Biological Chemistry, 277(5), 3303–3309.

53. Slepenkov, S. V., Darzynkiewicz, E., & Rhoads, R. E. (2006). Stopped-flow kinetic analysis of eIF4E and phosphorylated eIF4E binding to cap analogs and capped oligoribonucleotides: Evidence for a one-step binding mechanism. Journal of Biological Chemistry, 281(21), 14927–14938.

54. Antos, J. M., Truttmann, M. C., & Ploegh, H. L. (2016). Recent advances in sortase-catalyzed ligation methodology. Current Opinion in Structural Biology, 38(5), 111–118.

55. Popp, M. W. L., Antos, J. M., & Ploegh, H. L. (2009). Site-Specific protein labeling via UNIT 15.3 sortase-mediated transpeptidation. In Current Protocols in Protein Science (Issue SUPPL. 56).

56. Ton-That, H., Liu, G., Mazmanian, S. K., Faull, K. F., & Schneewind, O. (1999). Purification and characterization of sortase, the transpeptidase that cleaves surface proteins of Staphylococcus aureus at the LPXTG motif. Proceedings of the National Academy of Sciences, 96(22), 12424–12429.

57. Mao, H., Hart, S. A., Schink, A., & Pollok, B. A. (2004). Sortase-Mediated Protein Ligation: A New Method for Protein Engineering. Journal of the American Chemical Society, 126(9), 2670–2671.

58. Theile, C. S., Witte, M. D., Blom, A. E. M., Kundrat, L., Ploegh, H. L., & Guimaraes, C. P. (2013). Site-specific N-terminal labeling of proteins using sortase-mediated reactions. Nature Protocols, 8(9), 1800–1807.

59. Hirakawa, H., Ishikawa, S., & Nagamune, T. (2012). Design of Ca 2+ - independent Staphylococcus aureus sortase A mutants. Biotechnology and Bioengineering, 109(12), 2955–2961.

60. Schmohl, L., & Schwarzer, D. (2014). Sortase-mediated ligations for the site-specific modification of proteins. Current Opinion in Chemical Biology, 22, 122–128.

61. Sekar, R. B., & Periasamy, A. (2003). Fluorescence resonance energy transfer (FRET) microscopy imaging of live cell protein localizations. In Journal of Cell Biology (Vol. 160, Issue 5, pp. 629–633).

62. Bajar, B. T., Wang, E. S., Zhang, S., Lin, M. Z., & Chu, J. (2016). A guide to fluorescent protein FRET pairs. In Sensors (Switzerland) (Vol. 16, Issue 9). MDPI AG.

63. Piston, D. W., & Kremers, G. J. (2007). Fluorescent protein FRET: the good, the bad and the ugly. In Trends in Biochemical Sciences (Vol. 32, Issue 9, pp. 407–414).

64. Ryder, S. P., Recht, M. I., & Williamson, J. R. (2008). Quantitative analysis of protein-RNA interactions by gel mobility shift. *Methods in Molecular Biology*, *488*, 99–115.